Atmos. Meas. Tech., 10, 1783–1802, 2017
www.atmos-meas-tech.net/10/1783/2017/
doi:10.5194/amt-10-1783-2017

Atmospheric Measurement Techniques
Open Access
EGU

Optimizing observations of drizzle onset with millimeter-wavelength radars

Claudia Acquistapace[1], Stefan Kneifel[1], Ulrich Löhnert[1], Pavlos Kollias[2,1], Maximilian Maahn[3,4], and Matthias Bauer-Pfundstein[5]

[1]Institute for Geophysics and Meteorology, University of Cologne, Pohligstr. 3, 50969 Cologne, Germany
[2]Stony Brook University, Stony Brook, NY 11794-5000, USA
[3]Cooperative Institute for Research in Environmental Sciences, University of Colorado, 216 UCB, Boulder, CO 80309, USA
[4]Earth System Research Laboratory, National Oceanographic and Atmospheric Administration, 325 Broadway, Boulder, CO 80305, USA
[5]METEK Meteorologische Messtechnik GmbH, Fritz-Straßmann-Straße 4, 25337 Elmshorn, Germany

Correspondence to: Claudia Acquistapace (cacquist@meteo.uni-koeln.de)

Received: 25 September 2016 – Discussion started: 7 November 2016
Revised: 30 March 2017 – Accepted: 11 April 2017 – Published: 12 May 2017

Abstract. Cloud Doppler radars are increasingly used to study cloud and precipitation microphysical processes. Typical bulk cloud properties such as liquid or ice content are usually derived using the first three standard moments of the radar Doppler spectrum. Recent studies demonstrated the value of higher moments for the reduction of retrieval uncertainties and for providing additional insights into microphysical processes. Large effort has been undertaken, e.g., within the Atmospheric Radiation Measurement (ARM) program to ensure high quality of radar Doppler spectra. However, a systematic approach concerning the accuracy of higher moment estimates and sensitivity to basic radar system settings, such as spectral resolution, integration time and beam width, are still missing.

In this study, we present an approach on how to optimize radar settings for radar Doppler spectra moments in the specific context of drizzle detection. The process of drizzle development has shown to be particularly sensitive to higher radar moments such as skewness. We collected radar raw data (I/Q time series) from consecutive zenith-pointing observations for two liquid cloud cases observed at the cloud observatory JOYCE in Germany. The I/Q data allowed us to process Doppler spectra and derive their moments using different spectral resolutions and integration times during identical time intervals. This enabled us to study the sensitivity of the spatiotemporal structure of the derived moments to the different radar settings. The observed signatures were further investigated using a radar Doppler forward model which allowed us to compare observed and simulated sensitivities and also to study the impact of additional hardware-dependent parameters such as antenna beam width.

For the observed cloud with drizzle onset we found that longer integration times mainly modify spectral width (S_w) and skewness (S_k), leaving other moments mostly unaffected. An integration time of 2 s seems to be an optimal compromise: both observations and simulations revealed that a 10 s integration time – as it is widely used for European cloud radars – leads to a significant turbulence-induced increase of S_w and reduction of S_k compared to 2 s integration time. This can lead to significantly different microphysical interpretations with respect to drizzle water content and effective radius. A change from 2 s to even shorter integration times (0.4 s) has much smaller effects on S_w and S_k. We also find that spectral resolution has a small impact on the moment estimations, and thus on the microphysical interpretation of the drizzle signal. Even the coarsest spectral resolution studied, 0.08 ms^{-1}, seems to be appropriate for calculation moments of drizzling clouds. Moreover, simulations provided additional insight into the microphysical interpretation of the skewness signatures observed: in low (high)-turbulence conditions, only drizzle larger than 20 µm (40 µm) can generate S_k values above the S_k noise level (in

our case 0.4). Higher S_k values are also obtained in simulations when smaller beam widths are adopted.

1 Introduction

Millimeter wavelength (cloud) radars are a key component of ground-based remote sensing because of their ability to detect and penetrate most cloud types, thus providing range-resolved cloud structure. The number of cloud radars around the world and the range of their application in weather and climate research have experienced significant growth in the last 20 years (e.g. Kollias et al., 2007a; Illingworth et al., 2007; Löhnert et al., 2011; Görsdorf et al., 2015; Kollias et al., 2016). The majority of cloud radars installed worldwide are Doppler radars with the ability to record the full Doppler spectrum. The Doppler spectrum provides the distribution of target backscatter as a function of Doppler velocity and, when recorded in zenith-mode, it gives information about their vertical motion (Atlas et al., 1973). Commonly, Doppler spectra are not directly used but several moments are derived from them: the first two moments (equivalent radar reflectivity factor Z_e, mean Doppler velocity V_d) are most widely exploited while microphysical studies increasingly make use of higher moments such as spectral width (S_w), skewness (S_k) and kurtosis (e.g. Kollias et al., 2011a; Luke and Kollias, 2013; Maahn et al., 2015; Maahn and Löhnert, 2017).

Considering warm clouds, the formation of drizzle in stratocumulus clouds and the characterization of its signature in radar Doppler spectra has been of particular interest during the last decades. Gossard (1994), Frisch et al. (1995) and Gossard et al. (1997) developed retrieval techniques exploiting reflectivity, mean Doppler velocity and spectral width to derive drizzle and cloud drop size distributions. Cloud radar observations have also been combined with other remote sensors like microwave radiometers (e.g Frisch et al., 1995) and lidar (e.g O'Connor et al., 2005). Kollias et al. (2011a) showed the added value of higher radar moments like skewness and kurtosis for drizzle studies using forward simulations of radar Doppler spectra. They found that, in particular, the combined signatures of reflectivity and skewness are very sensitive to early drizzle formation. The theoretical findings have been confirmed by a detailed observational study (Kollias et al., 2011b) in which the authors also compared the observed vertical evolution of the signatures with drizzle simulations using a 1D bin microphysical model. In a follow-up study, Luke and Kollias (2013) developed a retrieval of drizzle particle size distribution based on the deconvolution of cloud and drizzle peak in regions where drizzle presence was identified by positive skewness.

Kollias et al. (2011a), Kollias et al. (2011b) and Luke and Kollias (2013) highlighted the importance of high-quality (artifact free) radar Doppler spectra collected with high spectral velocity resolution (Kollias et al., 2007b). The current generation of the US Department of Energy Atmospheric Radiation Measurements (ARM) program profiling W and Ka-band cloud radars use sampling strategies that enable the detection of microphysical signatures (Kollias et al., 2016). These strategies have been developed based on long-term experience and extensive data analysis for various cloud types. The majority of cloud radars installed across Europe are Ka-band systems of the type microwave radar (MIRA) manufactured by METEK GmbH (see Table 1) (Görsdorf et al., 2015). Their number strongly increased during the last 10 years, almost reaching the number of Ka-band radars deployed within the ARM program. Due to differences between the radar systems (e.g., radar beam width) it is not clear whether the settings found to be optimal within ARM are directly transferable to the MIRA systems. In this study, the requirements for high-quality radar Doppler spectra are explored for this new class of operating radars. The strategies developed to obtain the optimal settings can also potentially be applied to other radar systems.

The early detection of drizzle using the radar Doppler spectra skewness is used here as the target for this optimization. While the presented methodology can also be applied to other microphysical processes (for example, aggregation of ice crystals), we selected drizzle development because it is one of the most intensively studied applications using higher radar moments. Some of the relevant radar parameters necessary to capture signatures of drizzle development are hardware dependent. For example, a large radar beam width will increase the influence of dynamical broadening effects like turbulence or spectral artifacts caused by partial beam filling. Problems of partial beam filling will also occur when the observed cloud is thin with respect to the pulse length (Uttal and Kropfli, 2001). Other parameters, like the integration time or spectral resolution, can be adjusted by the user and their impact on the estimation of moments in the context of drizzle detection has never been assessed before.

The integration time specifies how many initially derived Doppler spectra are temporally averaged by the radar processing software to a single spectrum which is then stored and from which all further radar moments are derived. A longer integration time reduces data storage space and helps to improve the signal-to-noise ratio. At the same time, longer integration time results in the smearing of microphysical signatures due to small scale turbulence and radar-resolved vertical air motion (Kollias et al., 2005). The second critical parameter is the spectral resolution. The spectral resolution of the Doppler velocity is defined by

$$\Delta v = \frac{2v_N}{n_{fft}}, \quad (1)$$

where v_N is the Nyquist velocity and n_{fft} is the length of the discrete fast Fourier transform (FFT) used to produce the Doppler spectrum. A too-coarse spectral resolution might introduce biases in the moment estimation (uncertainties in dis-

Table 1. Current radar settings for various MIRA METEK systems.

Location	Institution	Integration time ΔT [s]	n_{fft}	PRF [kHz]	V_{N} [ms^{-1}]	Comments
Chilbolton (UK)	University of Leeds	10	512	7.5	15	
Cleveland (Ohio, USA)	NASA	10	256	5	10	
Galway (Ireland)	National University of Ireland (NUI)	10	256	5	10	
Hamburg (Germany)	Max Planck Institute (MPI)	10	256	5	10	
Iqaluit (Canada)	Environment Canada (EC)	1	256	5	10	
Jülich-JOYCE (Germany)	University of Cologne (IGMK)	1	256	5	10.6	
Karlsruhe, (Germany)	Karlsruhe Institute of Technology (KIT)	–	256	5	10	mainly used for campaigns
Kuopio (Finland) (before Helsinki and Sudankylä)	Finnish Meteorological Institute (FMI)	10	512	5	10	
Leipzig (Germany)	Leibniz Institute for Tropospheric Research (TROPOS)	10	256	5	10	1 s resolution stored for 5 days, for special events (defined by the radar users) moment data are reprocessed with 1 s resolution
Lindenberg (Germany)	Deutscher Wetterdienst (DWD)	10	256	5	10	
Munich (Germany)	Ludwig-Maximilian Universität München (LMU)	10	256	7.5	10	
Potenza (Italy)	Consiglio Nazionale delle RIcerche: istituto di Metodologie per l'Analisi Ambientale (CNR-IMAA)	10	256	5	10	
Huancayo (Peru)	Laboratorio de Microfísica Atmosférica y Radiación (LAMAR), Istituto Geofisico del Peru' (IGP)	10	128	5	10	
Zugspitze (Germany)	German Aerospace Center (DLR)	10	256	5	10	

crete integration) and can also be responsible for loss of specific microphysical signatures (e.g., the very narrow peak of supercooled liquid water in mixed-phase clouds). As can be seen in Table 1, the most widely used settings in the MIRA community for integration time and spectral resolution are 10 s and 0.08 ms^{-1} ($n_{\mathrm{fft}} = 256$). In contrast, the majority of cloud radars operated within the ARM program use a much smaller integration time of 2 s and a finer spectral resolution of 0.03 ms^{-1} ($n_{\mathrm{fft}} = 512$) (Kollias et al., 2005). Moreover, different antenna beam widths, 0.3 and 0.6°, are used in ARM and MIRA communities, respectively.

Considering the number of researchers working with both systems, it is important to address the question of whether such differences in radar hardware and sampling strategy affect the portability of retrievals algorithms from one cloud radar system to another. In order to answer this question, we recorded raw radar data (hereafter called I/Q data) of two shallow liquid clouds at the Jülich Observatory for Cloud Evolution (JOYCE) (Löhnert et al., 2015) which is described in Sect. 2. The clouds have been identified by the Cloudnet categorization algorithm (Illingworth et al., 2007) to be a nondrizzle and drizzle case. The collected I/Q data allowed us to derive Doppler spectra and moments with different integration times and spectral resolutions. By this, we were able to study the sensitivity of reflectivity (Z_{e}), mean Doppler velocity (V_{d}), spectral width (S_{w}) and skewness (S_{k}) to the different settings based on the identical raw data (Sect. 3). We further compared the observed sensitivities with results from experiments performed with a radar Doppler spectrum forward simulator assuming a range of dynamical and microphysical conditions that match retrieved turbulence parameters and our observed distribution of reflectivity and skewness and we used the simulator to also assess the impact of different radar beam widths. Concluding remarks are given in Sect. 4.

2 Data and methodology

2.1 Cloud radar

We analyzed two case studies of shallow liquid clouds observed at the Jülich Observatory for cloud evolution (JOYCE) (Löhnert et al., 2015), equipped with a Ka-band MIRA Doppler cloud radar (hereafter called JOYRAD-35) (Fig. 1). Due to its high sensitivity, it is well suited for the study of thin, low-reflectivity clouds such as nondrizzling and drizzling stratocumulus clouds which are often observed over JOYCE. JOYRAD-35 transmits linear polarized wave at 35.5 GHz and simultaneously receives the co- and cross-polarized backscattered signal. The antenna beam width is 0.6° and the range resolution is 30 m (an overview of the instrument specifications is provided in Table 2) over a given integration time. Observations in zenith mode are usually obtained at JOYCE with an integration time of 1 s and a 256 point FFT for generating the Doppler spectrum. JOYRAD-35 allows the number of FFT points to be changed from 256 to 512 and up to 1024. According to Eq. (1) and, given the Nyquist velocity of 10.625 ms^{-1}, we are able to realize spectral resolutions ranging from 0.08 ms^{-1} (standard settings) up to 0.02 ms^{-1}.

Figure 1. Scanning Ka-band Doppler cloud radar JOYRAD-35 (JOYRAD-35 system) installed at the JOYCE site, Jülich, Germany. Technical specifications of the radar are provided in Table 2.

2.2 Raw data processing and moment estimation

The JOYRAD-35 raw radar data processing is similar to the method described in Doviak and Zrnic (2014). The raw I/Q time series are converted into Doppler spectra from which the final Doppler spectrum is generated by averaging the raw spectra over a given integration time (see Table 3). This procedure is exemplarily illustrated in Fig. 2 for the I signal for a thin liquid cloud described in the following sections. Raw I/Q data are usually not stored because of their immense data volume (a raw file containing 1 min of I/Q observations results in a file of 1.2 GB size). For this study we recorded the original I/Q data in order to analyze the sensitivity of the spectra and their moments to different n_{fft} and integration times ΔT while using identical raw data. However, due to data storage limitations we had to restrict the maximum length of the recorded data to 4 min.

The raw I/Q data were processed using $n_{\mathrm{fft}} = 256$, 512, 1024 and three different integration times $\Delta T = 0.4$, 2, 10 s. A different number of radar Doppler spectral averages was used for different n_{fft} in order to achieve the final Doppler spectrum for one of the selected ΔT (Table 4). Only spectra within the cloud boundaries as identified by the Cloudnet classification algorithm were analyzed. We used the procedure described in Hildebrand and Sekhon (1974) to estimate the radar Doppler spectra noise floor (mean and peak value). The radar moments were calculated by subtracting peak noise level from the averaged spectrum $\hat{S}(v)$ of the Doppler velocity v (in ms^{-1}) using the following expressions

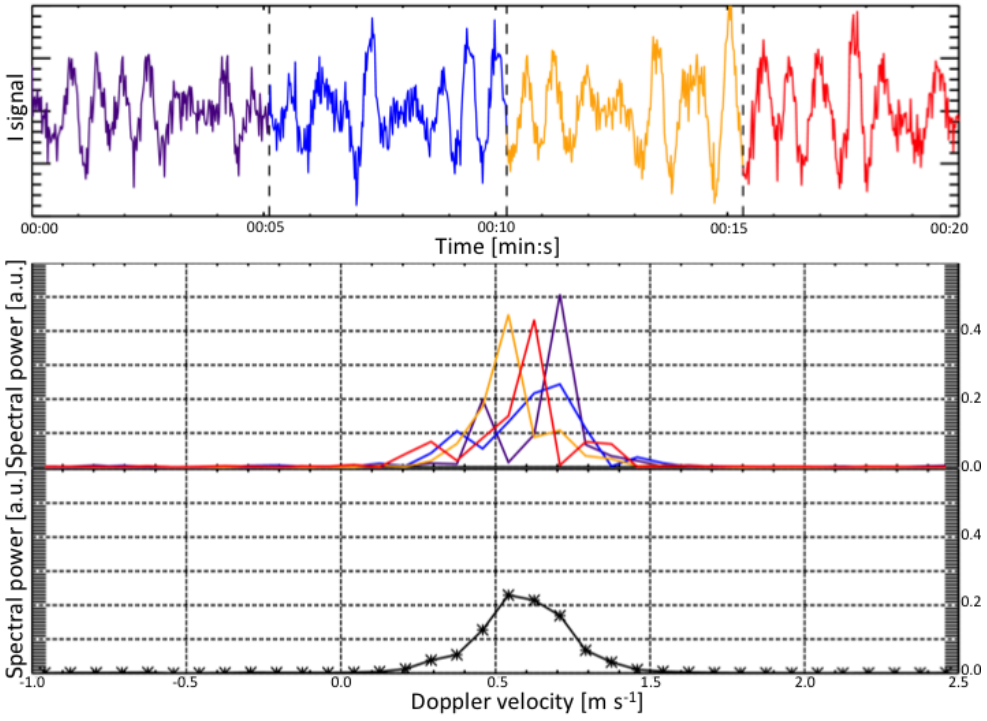

Figure 2. Illustration of the standard procedure for deriving radar Doppler spectra from raw I/Q time series (see also detailed description of the method in Doviak and Zrnic, 2014). The upper panel shows a time series of 1024 in-phase (I) samples (Q time series not shown); the different colors denote four 256 point long subsamples which are used in combination with the corresponding Q samples to perform a 256 FFT resulting in the raw Doppler spectra shown in the panel below. Each raw spectrum corresponds to an integration time of $(0.0512\,s)$. The lowest panel shows the average of the four raw spectra corresponding to a total integration time of 0.2 s.

Table 2. Current radar settings for JOYRAD35 system at JOYCE, Jülich (DE).

Parameter	Specification	Comments
Frequency	35.5 GHz	corresponding to wavelength of 8.5 mm
Peak power (max)	25 kW	
Average power	24 W	
Pulse width	200 ns	adjustable (100, 200, or 400 ns)
Pulse repetition frequency	5 kHz	adjustable (5–10 kHz)
Minimum height	150 m	full sensitivity above 400 m
Measuring range	15 km	adjustable (7.5–30 km)
Range resolution	30 m	adjustable (15, 30, or 60 m)
3 dB one-way antenna beam width in the E and H planes	0.6°	
Doppler velocity resolution	0.025 m s^{-1}	depends on FFT length
Nyquist velocity	±10.6 m s^{-1}	
Maximum sensitivity at 5 km (integration 0.1 s)	−45 dBZ	
Calibration system accuracy	±0.5 dB	
Number of gates (with simultaneous stored raw data)	500	
Number of averaging spectra	200	adjustable (1–32768)
Manufacturer	Metek	

(e.g. Kollias et al., 2011a). First, the radar Doppler spectrum $\hat{S}$ is converted from SI units to S in mm^6 s m^{-4} with

$$S(v) = 10^{18} \frac{\lambda^4}{|K_w|^2 \pi^5} \hat{S}(v), \quad (2)$$

Table 3. Minimum integration time taken to generate a single raw Doppler spectrum for each selected spectral resolution.

256 fft length/spectral res. ($\Delta v = 0.08\,\mathrm{ms}^{-1}$)	512 fft length/spectral res. ($\Delta v = 0.04\,\mathrm{ms}^{-1}$)	1024 fft length/spectral res.($\Delta v = 0.02\,\mathrm{ms}^{-1}$)
0.0512 s	0.1 s	0.2 s

Table 4. Number of averaged spectra to obtain each integration time for different n_{fft} cases.

Integration time $\Delta T[s]$	$N^{256}_{\mathrm{spectra}}$	$N^{512}_{\mathrm{spectra}}$	$N^{1024}_{\mathrm{spectra}}$
0.4 s	8	4	2
2 s	40	20	10
10 s	200	100	50

where $|K_{\mathrm{w}}|^2$ is related to the refractive index of liquid water and λ is the radar wavelength in meters. Commonly, $|K_{\mathrm{w}}|^2$ is fixed to 0.93 (default value in MIRA processing).

Then, the equivalent radar reflectivity factor Z_{e} (zeroth moment, hereafter called reflectivity) in $\mathrm{mm}^6\,\mathrm{m}^{-3}$ can be obtained with

$$Z_{\mathrm{e}} = \int_{-v_{\mathrm{N}}}^{v_{\mathrm{N}}} S(v)\mathrm{d}v\,. \tag{3}$$

The mean Doppler velocity V_{d} in ms^{-1} is related to the first moment of the Doppler spectrum and defined as

$$V_{\mathrm{d}} = \frac{1}{Z_{\mathrm{e}}} \cdot \int_{-v_{\mathrm{N}}}^{v_{\mathrm{N}}} S(v) \cdot v\mathrm{d}v. \tag{4}$$

Z_{e} represents the integral of the spectrum within the Nyquist velocity range. For Rayleigh scatterers, Z_{e} is equal to the reflectivity factor Z, which is defined as the sixth moment of the drop size distribution (DSD) (Doviak and Zrnic, 2014). V_{d} is the reflectivity weighted mean velocity of the scattering particles relative to the radar. The radar spectral width in ms^{-1} is related to the second moment of $S(v)$ and defined as

$$S_{\mathrm{w}} = \sqrt{\frac{1}{Z_{\mathrm{e}}} \cdot \int_{-v_{\mathrm{N}}}^{v_{\mathrm{N}}} S(v) \cdot (v - V_{\mathrm{d}})^2\mathrm{d}v}. \tag{5}$$

S_{w} represents the variance of the hydrometeor's motions. In absence of vertical air motion and turbulence, it only depends on the variability of terminal fall velocities within the radar volume and hence reflects the width of the DSD of the precipitating drops. Air motion can additionally broaden the spectrum and enhance S_{w}. A comprehensive description of broadening effects can be found in Doviak and Zrnic (2014).

The skewness S_{k} (dimensionless) provides the degree of asymmetry of a distribution and, when applied to a Doppler spectrum, it describes its degree of asymmetry, namely the degree of inclination of the peak of the spectrum that represents situations in which the peak is tilted to the left or to the right (Maahn, 2015). Its value is determined by the entire Doppler spectrum and it can also be affected by asymmetries in the tails of the shape. A Gaussian peak has a skewness of zero, but it should be noted that in theory an asymmetric spectrum can also have zero skewness if the two parts of the spectrum compensate each other. However, in reality, this case is very rarely observed. Most of the times in drizzling/nondrizzling applications, S_{k} helps to detect deviations from the symmetric, mostly Gaussian shape observed in nondrizzling Doppler spectra. The mathematical expression for the skewness is

$$S_{\mathrm{k}} = \frac{1}{Z_{\mathrm{e}} \cdot (S_{\mathrm{w}})^3} \int_{-v_{\mathrm{N}}}^{v_{\mathrm{N}}} S(v) \cdot (v - V_{\mathrm{d}})^3\mathrm{d}v. \tag{6}$$

The sign of S_{k} depends on the sign convention adopted for the Doppler velocity. In this study, we adopted the convention of velocities being positive when moving towards the radar (downwards) which results in positive S_{k} values occurring when the spectrum shows an asymmetry towards positive velocities (e.g., to the right of the main peak in Fig. 2). S_{k} as well as S_{w} are of particular interest for studying drizzle growth, as revealed by former studies (Luke and Kollias, 2013; Kollias et al., 2011a, b).

2.3 Nondrizzle and drizzle datasets

Two 4 min-long I/Q time series from stratiform thin liquid clouds classified by the Cloudnet algorithm to be nondrizzle and drizzle clouds were analyzed. The nondrizzle case was recorded at JOYCE on 20 November 2014 between 12:00 and 13:00 UTC. The thin cloud layer was located between 300 and 500 m above ground (Fig. 3). The liquid water path (LWP) derived from the collocated microwave radiometer only reached values up to $50\,\mathrm{gm}^{-2}$. The time–height structure of S_{w} processed for the three different spectral resolutions (n_{fft}) and integration times (ΔT) is shown in the lower panels of Fig. 3. A longer integration time smooths the microphysical and dynamical structures and results in an increase of S_{w} with longer ΔT. On the other hand, the spectral resolution has only a minor effect on the derived S_{w} and the effects of the different settings on the reflectivity and S_{k} field (not shown) are small. Also, a decrease of the cloud thickness is mostly observed when integration time is changed from 2 to 0.4 s. The sensitivity of the radar becomes smaller when shorter integration times are used which has a strong impact on the cloud edge detection. The lowest cloudy range gate identified in the 2 and 10 s integration time at 270 m is almost completely missed when the 0.4 s integration time is used.

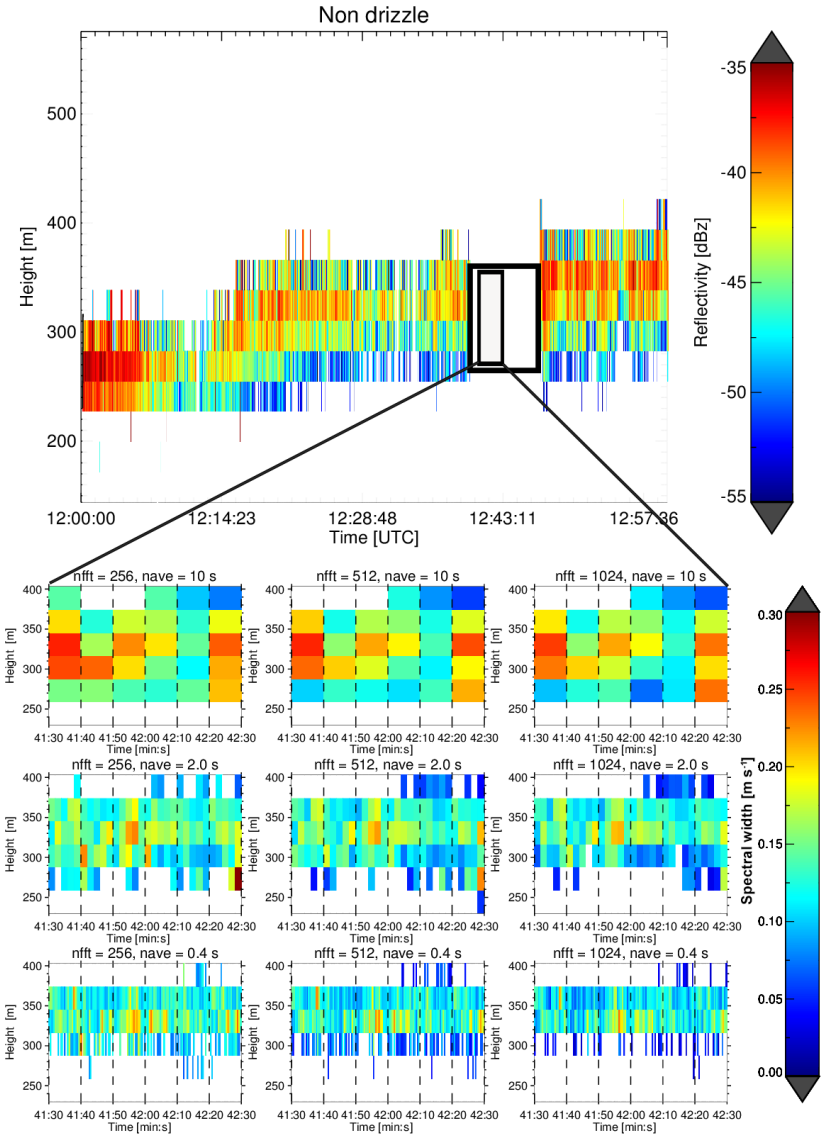

Figure 3. Time–height plot composite of reflectivity and spectral width for the nondrizzle case on 20 November 2014. The larger upper panel shows the reflectivity for the entire 1 h period obtained with standard radar settings of nfft = 256 and $\Delta T = 1$ s; the larger black box denotes the 4 min time period of I/Q data recording. The lower subplots show time–height plots of a 1 min time period (small black box) of spectral width for three different integration times (decreasing from top to bottom) and spectral resolutions (increasing from left to right).

The time series of a drizzle event was recorded on 24 June 2015 between 09:00 and 10:00 UTC (Fig. 4). The drizzling cloud first appeared at nighttime and its cloud boundaries ranged between 700 and 1000 m. The Cloudnet classification identified this cloud as drizzling until approximately 09:00 UTC. When the I/Q data were recorded, drizzle was ending over JOYCE and the cloud disappeared within the following hours. LWP decreased from the highest values observed in the morning (200 $\mathrm{g\,m^{-2}}$) to values of 93 $\mathrm{g\,m^{-2}}$ during the I/Q collection period.

Compared to the nondrizzle case (Fig. 3), the presence of drizzle is clearly indicated in the 10 dB larger reflectivities and enhanced positive S_k up to 1.5 (Fig. 4). Unlike the nondrizzling case, the higher radar moments like S_k, in particular, are now revealing greater sensitivity to the radar settings. The spectral resolution (as indicated by the changing n_{fft}) has a relatively small effect on the temporal-spatial structure of S_k. The variability of S_k appears to be best captured with 2 s integration time while extreme values and structure are lost when using 10 s integration time. A smaller value of 0.4 s seems not to provide more structure but rather to increase the noise. Both in the nondrizzle and drizzle cases, a much larger smearing effect is found when changing from 2 to 10 s averaging time compared to moving from 0.4 to 2 s. While this

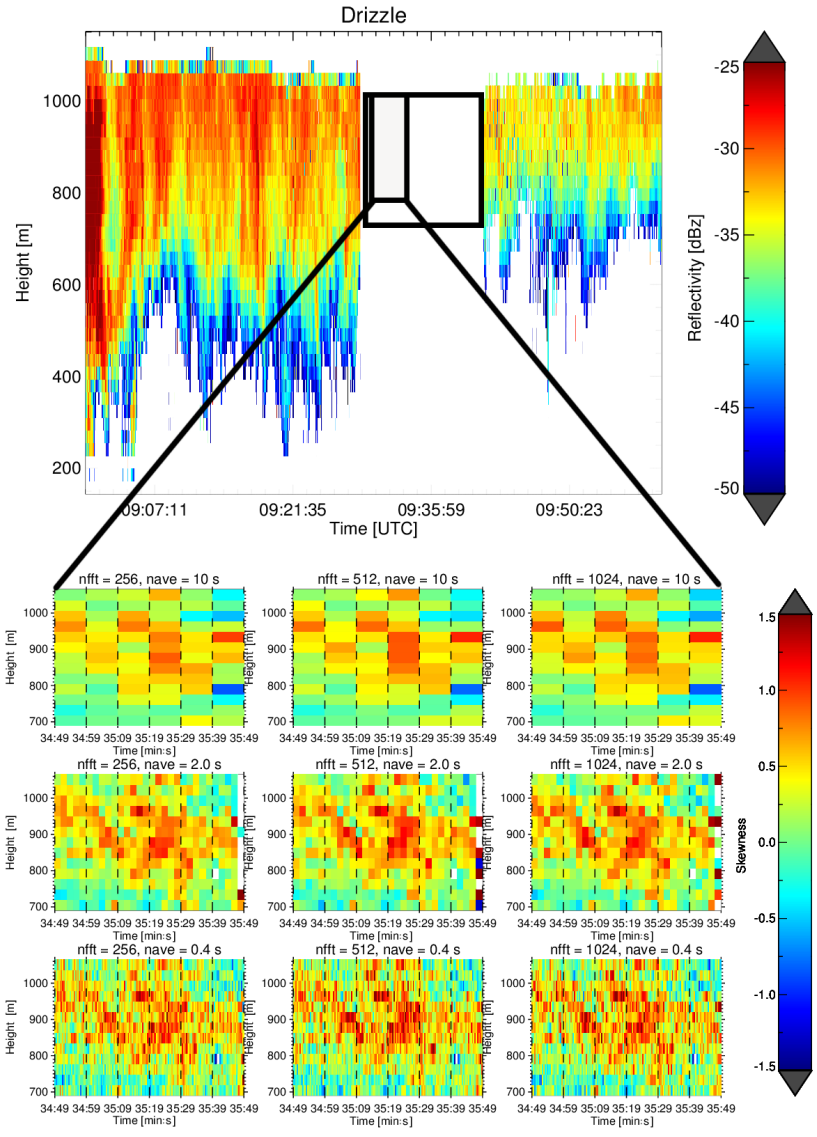

Figure 4. Similar to Figure 3 but for the drizzle case on 24 June 2015. In this case, the subplots show skewness instead of spectrum width.

effect is certainly connected to the scales of variability of the underlying cloud structures, it is noteworthy because the majority of cloud radars across Europe use 10 s integration time. However, the ARM program uses a typical integration time for cloud radars of 2 s. One question we aimed to address with this study is whether this is relevant only for specific case studies or whether such discrepancies in radar settings might also have implications on the derived radar moment statistics, which may affect the quality of evaluations of drizzle parameterizations in numerical models.

2.4 Radar forward simulator

The observed radar Doppler spectra are affected by the underlying microphysics as well as by dynamical effects such as turbulence. In reality, a complete separation of both effects is often a challenging task (Tridon and Battaglia, 2015). The limitations for storing the large amounts of raw I/Q data also limited the total observed time of drizzle clouds. To analyze the effects of dynamics and microphysics separately, but also to investigate whether the observed drizzle signatures are consistent with commonly used assumptions about drizzle microphysics, we performed forward simulations of radar Doppler spectra and their corresponding moments using the radar forward simulator included in the Passive and Active Microwave radiative TRAnsfer (PAMTRA) framework (Maahn, 2015). The radar operator implemented in PAMTRA is similar to the radar simulator described in Kollias et al. (2014). Mie scattering (Mie, 1908) is used to estimate the backscattering properties, then the approach of

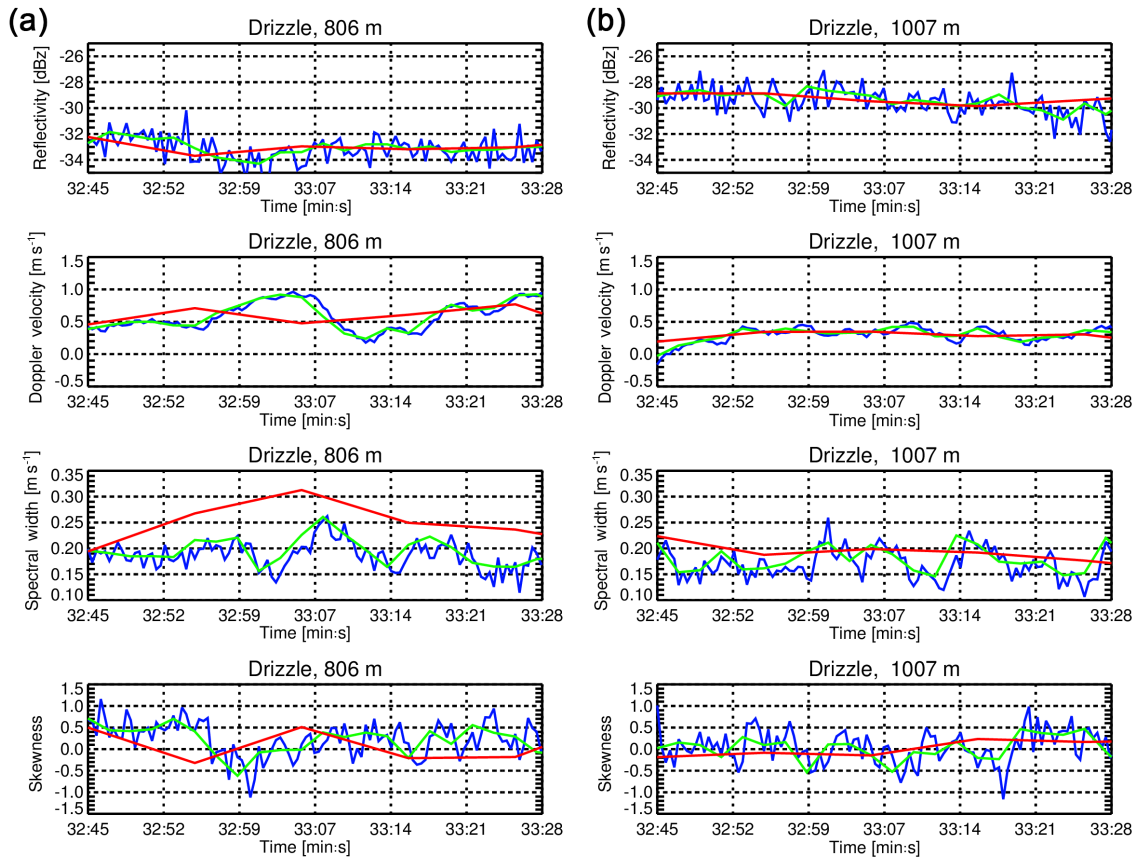

Figure 5. Example time series of the first four Doppler moments obtained from altitudes close to cloud top **(b)** and close to cloud base **(a)** for drizzle case on 24 June 2015 (see Fig. 4). Different colors correspond to different integration times of 10 s (red), 2 s (green) and 0.4 s (blue); n_{fft} is 512 for all time series.

Khvorostyanov and Curry (2002) is used to assign the corresponding fall velocity to every size bin. Finally, turbulence is convoluted and noise is applied in agreement with the MIRA characteristics (Zrnic, 1975). The moments of the synthetic Doppler spectra are derived in the same way as for the observations. Input variables for PAMTRA include the DSD of cloud and drizzle populations, radar instrument parameters like antenna beam width, n_{fft} and ΔT as well as vertical air motion and eddy dissipation rate (EDR).

3 Results and discussion

In this section, the impact of different integration times and spectral resolutions on the derived radar moments using the collected I/Q datasets for nondrizzle and drizzle clouds is analyzed. The observations are subsequently compared to the radar forward simulations in order to assess the impact of different n_{fft} and ΔT on identifying drizzle growth signatures under different turbulence conditions.

3.1 Observed impact of integration time and spectral resolution

3.1.1 Impact of integration time on individual time series of radar moments

The impact of different integration times on the radar moments is illustrated in Fig. 5. Time series of the four radar moments are shown for the drizzle case close to cloud base at 806 m (right column in Fig. 5) and close to cloud top at 1007 m (left column in Fig. 5).

Varying the integration time has little effect on the mean recorded radar reflectivity values. The absolute Z_{e} differences between values derived with different integration times vary randomly within 2 dB. This is what we expect from a reflectivity field with relatively low temporal variability. Signatures due to microphysical processes affecting the shape of the spectrum are less relevant for Z_{e} because it is the integral of the spectrum. Larger effects of different integration times are found for V_{d}, particularly between the 10 s and the two shorter integration times. While the differences at cloud top are relatively small, V_{d} values at cloud base obtained with

10 s integration time sometimes deviate up to 50 % from the values derived with 2 and 0.4 s. The variability of vertical motions in this case is larger at cloud base and hence, the effect of different averaging times is also more pronounced. The effect of averaging times increases for higher radar moments which are in general more sensitive to the shape and tails of the spectrum. Hence, not only do the temporal variability of the microphysical processes become relevant but so do the effect of air motion and turbulence smoothing the microphysical signatures of the individual spectra. The spectrum width increases with longer integration times because narrow individual spectra, which are shifted due to vertical air motions, are averaged together; this also results in a more symmetrical shape of the average spectrum and hence skewness values are closer to zero (Luke and Kollias, 2013). It is noteworthy that for all radar Doppler spectra moments, only small differences are found between the 2 and 0.4 s integration time but differences increase drastically when using 10 s. At least for drizzle studies, integration times equal to or shorter than 2 s should be preferred for capturing small-scale vertical motions and to ensure high quality of higher moments (S_w, S_k) of the Doppler spectrum.

The nondrizzle case is used as a benchmark for the statistical variance of the radar measurements. In nondrizzling conditions, the radar Doppler spectrum is dominated by turbulence (Kollias et al., 2001) and the impact of microphysics on the shape of the radar Doppler spectrum is negligible. Assuming that skewness in these cases is close to zero, we derived the variability of skewness due to instrumental noise and dynamical effects. Standard deviations of the skewness time series in the nondrizzling cloud using 2 s integration time and spectral resolutions of 256, 512 and 1024 range between 0.389 and 0.369 with a mean value over the three cases of 0.379. These values provide a threshold to detect the drizzle onset signatures from the noise caused by the fluctuations induced by the natural variability of the skewness in the presence of cloud droplets only.

3.1.2 Impact of signal-to-noise ratio and integration time on moment distributions

The observed normalized probability density functions of all radar Doppler spectra moments for the three integration times, and three n_{fft} are shown for the drizzling case and for the nondrizzling case in Fig. 6. For the nondrizzle case, the distributions of Fig. 6 (in detail in Fig. S1 in the Supplement) mainly show an expected increase in radar sensitivity and a shift in S_w towards larger values with longer integration time. The low spectral width and the low signal-to-noise ratio of the nondrizzle spectra causes the spectra to be rather noisy. Higher moments like S_k are more affected by the low signal-to-noise conditions, which explains the relatively broad S_k distribution. Our analysis focused mainly on the drizzle case shown in Fig. 6 in order to capture the effects that the radar settings can have in the presence of drizzle. Moreover, higher signal-to-noise conditions during drizzling conditions were expected to limit the influence of noise on the derived distributions. The presence of drizzle is visible in the distributions of radar moments: in comparison to the nondrizzle case (see Table 5), Z_e values are increased by about 10 dB and the mean Doppler velocity also peaks at about 0.25 ms^{-1} (see Table 6). Furthermore, the distribution of higher moments shows typical signatures of drizzle with S_w values larger than 0.06 ms^{-1} compared to the nondrizzle observations. The skewness values reveal the typical transition from almost zero values in the nondrizzle case to positive values with a mean around 0.25, indicating an asymmetry of the spectrum towards larger fall velocities due to larger drizzle particles; these signatures are in general agreement with former studies (e.g. Kollias et al., 2011a). The S_w values are considerably increased for the 10 s integration time while the shift is small for the two smaller integration times. The mean of the S_k distributions slightly decreases due to longer integration times (Table 6) which can again be explained by the more symmetrical shape of the spectra obtained using a longer integration time. While variations of spectral resolution produce random fluctuations towards both larger and smaller mean S_k values, reducing the integration times leads to a consistent increase in the mean skewness. This can be seen in Fig. 6, where the largest values found in the positive S_k region are decreasing for longer integration times. A similar but weaker effect can be found for the most positive V_d which we explain with relatively narrow regions within the cloud layer that already developed a larger amount of drizzle compared to the surrounding cloud layer. In light of early detection of drizzle onset regions, a 10 s integration time seems to be insufficient. The differences obtained in the skewness distributions can impact the ability to detect positive skewness signals induced by drizzle. Luke and Kollias (2013) showed S_k time series where the highest observed values of skewness reach up to 1.5. A reduced ability in detecting such extreme values due to longer integration times (for example with 10 s integration time, the maximum value observed is 1) can affect the potential to disentangle the low-frequency variability induced by the microphysics and the high-frequency variability due to noisiness and partial beam filling.

3.1.3 Impact of spectral resolution on moment distributions

For relatively narrow spectra, as they are found in clouds with no or little drizzle production, the spectral resolution might be of relevance for the quality of the derived moments. The spectral resolution could affect the quality of integral values such as reflectivity if a narrow spectrum – e.g., due to cloud droplets – is only resolved with a few spectral bins. A larger impact is expected for higher moments in which the spectral shape becomes important and hence spectral resolution potentially smoothes out spectral features. In order to investigate these potential effects of spectral resolution on

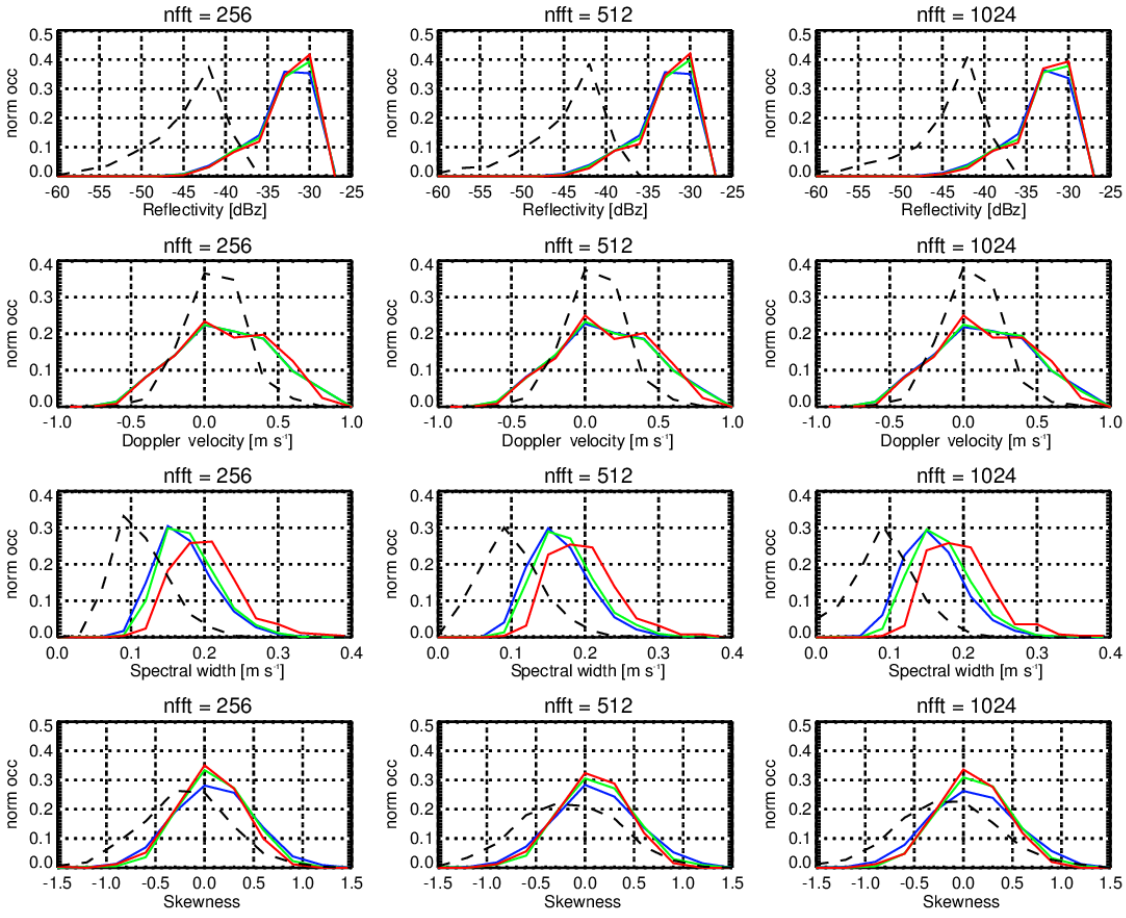

Figure 6. Distributions of radar moments for the drizzle case on 24 June 2015 (Fig. 4). The total number of values used for the different pdfs ranges between 252 for the 10 s integration time and 6174 for the 0.4 s integration time. Different colors in each plot correspond to different integration times of 10 s (red), 2 s (green) and 0.4 s (blue). The spectral resolution (nfft) increases from left to right; radar moments are from the top to the bottom row: reflectivity (Z_e), mean Doppler velocity (V_d), spectral width (S_w) and skewness (S_k). The black dashed line represents the corresponding distribution obtained in the nondrizzle case (20 November 2014) using 0.4 s averaging time (see Fig. S3).

Table 5. Mean distributions: 20 November 2014.

Moments	Integration time $\Delta T[s]$	nfft = 256	nfft = 512	nfft = 1024
Reflectivity	0.4 s	−43.0	−43.3	−43.1
	2.0 s	−44.5	−45.0	−45.0
	10 s	−46.0	−46.0	−46.1
Mean Doppler Velocity	0.4 s	0.17	0.17	0.16
	2.0 s	0.16	0.16	0.14
	10 s	0.17	0.17	0.21
Spectral width	0.4 s	0.13	0.11	0.11
	2.0 s	0.15	0.16	0.13
	10 s	0.17	0.16	0.15
Skewness	0.4 s	−0.04	−0.01	−0.005
	2.0 s	−0.04	0.01	−0.1
	10 s	−0.08	−0.07	−0.06

Table 6. Mean distributions: 24 June 2015.

Moments	Integration time $\Delta T[s]$	nfft = 256	nfft = 512	nfft = 1024
Reflectivity	0.4 s	−31.7	−31.8	−31.9
	2.0 s	−31.6	−31.6	−31.7
	10 s	−31.5	−31.5	−31.5
Mean Doppler velocity	0.4 s	0.25	0.26	0.26
	2.0 s	0.26	0.26	0.26
	10 s	0.26	0.26	0.26
Spectral width	0.4 s	0.19	0.18	0.18
	2.0 s	0.21	0.20	0.20
	10 s	0.22	0.21	0.21
Skewness	0.4 s	0.24	0.26	0.25
	2.0 s	0.25	0.24	0.27
	10 s	0.21	0.23	0.23

Table 7. Bias and standard deviation of the difference of moments derived from corresponding spectra with different spectral resolutions.

Nondrizzle	BIAS		STD		Drizzle	BIAS		STD	
	256 − 512	512 − 1024	256 − 512	512 − 1024		256 − 512	512 − 1024	256 − 512	512 − 1024
Z_e	0.28	0.32	0.89	1.16	Z_e	0.02	0.06	0.42	0.46
V_d	0.001	−0.006	0.08	0.12	V_d	−0.0011	−0.0009	0.05	0.04
S_w	0.013	0.011	0.04	0.03	S_w	0.007	0.003	0.02	0.02
S_k	−0.004	−0.006	0.31	0.39	S_k	−0.017	0.005	0.16	0.18

the different moments, we derived the Doppler spectra for all heights with 256, 512 and 1024 n_{fft}. The integration time for all n_{fft} was kept constant (2 s) to ensure that the spectra are based on identical time series of raw I/Q data and hence they contain identical information about dynamics and cloud microphysics. The bias and standard deviations (STD) of the scatter plots (Fig. S2 and S3) of $n_{fft} = 256$ versus 512 and 512 versus 1024 for the drizzle and the nondrizzle case are summarized in Table 7. In summary, the impact of different spectral resolutions is surprisingly small compared to the natural variability of the various moments shown in Fig. 5. The largest biases and STD are found for the nondrizzle case with values up to 0.3 dB for reflectivity, but those can still be considered negligible for most applications. The larger deviations in the nondrizzle case are attributed to the insufficiently resolved narrow spectra which lead to uncertainties in the estimate of the integral and spectral shape. Narrow nondrizzling cloud spectra are often represented by only a few spectral bins when using a spectral resolution of 0.08 ms^{-1} ($n_{fft} = 256$), for example in MIRA systems (Table 1). Such a coarse resolution also affects higher moments like S_w and S_k. In the drizzle case, the spectra are broader and sufficiently resolved even with the coarsest spectral resolution.

The distributions of all radar Doppler spectra moments for the three different integration times, and three n_{fft} for the drizzling case (Fig. 6) and nondrizzling case (Fig. S1) allow a closer examination of the reasons for the mismatches. Spectral resolution seems to have negligible influence on the distributions of Z_e and V_d (see Fig. 6). Table 7 summarizes the effects of spectral resolution and reveals that their impact is generally small even for the higher moments. The coarsest spectral resolution using $n_{fft} = 256$ is found to be sufficient to properly capture the typical signatures of drizzle onset.

3.2 Comparison with radar forward simulations

In this section we compare the results found in our observations with radar forward simulations using PAMTRA (see Sect. 2.4) to better understand the drizzle signatures and compare the effects of distinct radar parameters. The main goal of the simulations is to derive a range of possible microphysical and dynamical conditions which lie within the observed range of radar moments. This helps us prove that the observed differences due to radar settings are significant for identifying drizzle onset. In addition, it supports us in overcoming one main limitation of our observations: that they are based on relatively short time periods. The simulations further allow us to separately analyze the effects of turbulence and vertical air motion, which are input parameters for PAMTRA, from the microphysics when observed with different n_{fft} and ΔT.

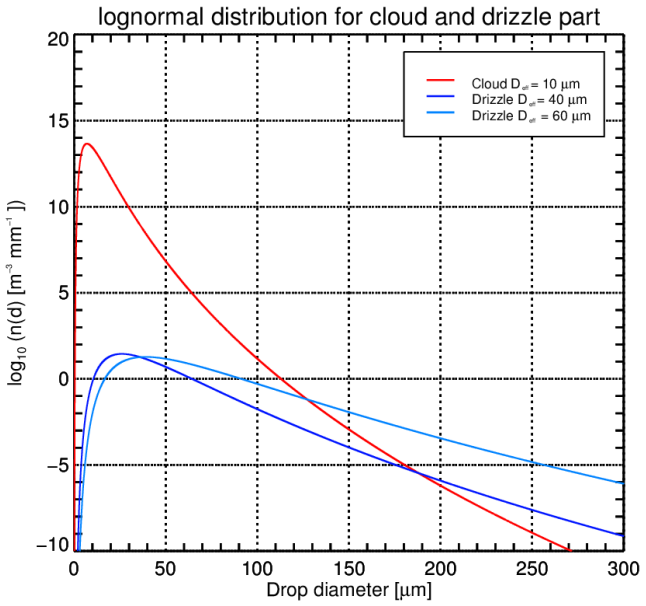

Figure 7. Drop size distributions used for radar forward simulations of the drizzle case. A single lognormal size distribution (red) is used for cloud droplets. For drizzle lognormal distributions with fixed $r_{\mathrm{LWC}} = 0.5\,\%$ and two different effective diameters are used: 40 µm (dark blue) and 60 µm (blue). The total number concentration N_{d} of the drizzle distribution is determined based on the other parameters according to Eq. (7).

3.2.1 Simulation setup

For the cloud droplet and drizzle components we assume a lognormal DSD of the form

$$N(D) = \frac{N_0}{\sqrt{2\cdot\pi}\,\sigma\,D}\exp\left[\frac{-\log(\frac{D}{D_0})^2}{2\sigma^2}\right], \tag{7}$$

where N_0 is the total number concentration (cm^{-3}), D_0 is the median diameter in meters, which is related to the effective diameter (D_{eff}) by $D_0 = D_{\mathrm{eff}}\exp\left[-\frac{5}{2}\sigma^2\right]$ (Miles et al., 2000). The effective diameter is connected to the effective radius R_{eff} by the relation $D_{\mathrm{eff}} = 2\times R_{\mathrm{eff}}$. Similar to Miles et al. (2000), we use for cloud droplets an effective radius $R_{\mathrm{eff,c}} = 5.4\,\mu\mathrm{m}$, $\sigma_{\mathrm{c}} = 0.35$ and total number concentration $N_0 = 300\,\mathrm{cm}^{-3}$. With these assumptions, we obtain a LWC for the cloud droplet component of $\mathrm{LWC_c} = 0.137\,\mathrm{gm}^{-3}$. This LWC is very close to the LWC of $0.133\,\mathrm{gm}^{-3}$ which we obtain in the drizzle case when we divide the average LWP obtained by the MWR by the average geometrical thickness of the cloud layer. We assume that the LWC due to drizzle ($\mathrm{LWC_d}$) is much smaller than $\mathrm{LWC_c}$ which is a common assumption in simulations of drizzle onset. In Frisch et al. (1995), the LWC ratio derived from the standard parameters used to discriminate between cloud and drizzle is 5 %, while in O'Connor et al. (2005), drizzle LWPs are often 2 orders of magnitude lower than cloud LWPs. For the simulations, we vary the LWC ratio (r_{LWC}) defined as $r_{\mathrm{LWC}} = \frac{\mathrm{LWC_d}}{\mathrm{LWC_c}}$ between 0.1 and 5 %. For the lognormal drizzle DSD, we use $\sigma_{\mathrm{d}} = 0.35$ (Frisch et al., 1995) and vary the drizzle effective radius $R_{\mathrm{eff,d}}$ from 10 to 60 µm. The drizzle number concentration N_{d} is then calculated based on the selected r_{LWC}. The DSDs for cloud droplets and drizzle are shown in Figure 7.

We derive distributions of eddy dissipation rate (EDR) and V_{d} for the 1 h period before the I/Q recording in order to obtain observational constraints for turbulence and vertical air motion which are needed as input to the radar forward simulations. EDR values are derived with an FFT method of V_{d} time series, similarly to the method described in Borque et al. (2016) which revealed a mean EDR of $3\times10^{-4}\,\mathrm{m}^2\,\mathrm{s}^{-3}$ and a standard deviation of $1.3\times10^{-4}\,\mathrm{m}^2\,\mathrm{s}^{-3}$. We also use the observed statistics of V_{d} as a first-order approximation for the vertical air motion. We derive a mean value of $0.43\,\mathrm{ms}^{-1}$ and a standard deviation of $0.39\,\mathrm{ms}^{-1}$; due to the nonnegligible terminal velocity of the drizzle component, the true air motion is likely to be smaller.

Simulated spectra for $r_{\mathrm{LWC}} = 2\,\%$ and $R_{\mathrm{eff,d}} = 20\,\mu\mathrm{m}$, $r_{\mathrm{LWC}} = 0.5\,\%$ and $R_{\mathrm{eff,d}} = 30\,\mu\mathrm{m}$ (to simulate different stages of drizzle onset) and EDR, representing the mean ($3\times10^{-4}\,\mathrm{m}^2\,\mathrm{s}^{-3}$) and largest values ($5\times10^{-3}\,\mathrm{m}^2\,\mathrm{s}^{-3}$) observed are shown exemplarily in Fig. 8. We interpret the first scenario as an early drizzle onset and the second scenario as a more developed stage of drizzle. For $R_{\mathrm{eff,d}} = 20\,\mu\mathrm{m}$, the convoluted spectrum is dominated by the cloud droplet peak even for low-turbulence conditions. When the $R_{\mathrm{eff,d}}$ is increased to 30 µm, the contribution of the drizzle grows to almost reach the cloud peak and causes the spectrum to become positively skewed. Increasing the EDR in general leads to a smoothing and symmetrical broadening of the spectrum, but the overall asymmetry due to drizzle is still clearly visible. A comparison of our simulations with observed spectra from regions where we interpret nondrizzle and drizzle growth (Fig. 8) shows an overall good agreement in terms of spectral shape, Z_{e} and S_{k}.

In order to take into account the effects of turbulence and changes in vertical velocity on the distribution of the Doppler spectra moments, we utilize the same microphysical scenarios described above. For each scenario, we run 1000 PAMTRA simulations, randomly choosing the noise and a pair of values of EDR and vertical air motion (V_{d}) based on the observed distributions. By doing this, we derive for each simulated spectrum statistically plausible air motion conditions (turbulence and vertical wind) which we expect to be close to the observations. The simulations are repeated for the three n_{fft} and ΔT in order to derive distributions of radar moments similar to our observations (Fig. 6). The desired ΔT is obtained in the simulations by averaging the same amount of Doppler spectra as in the observations.

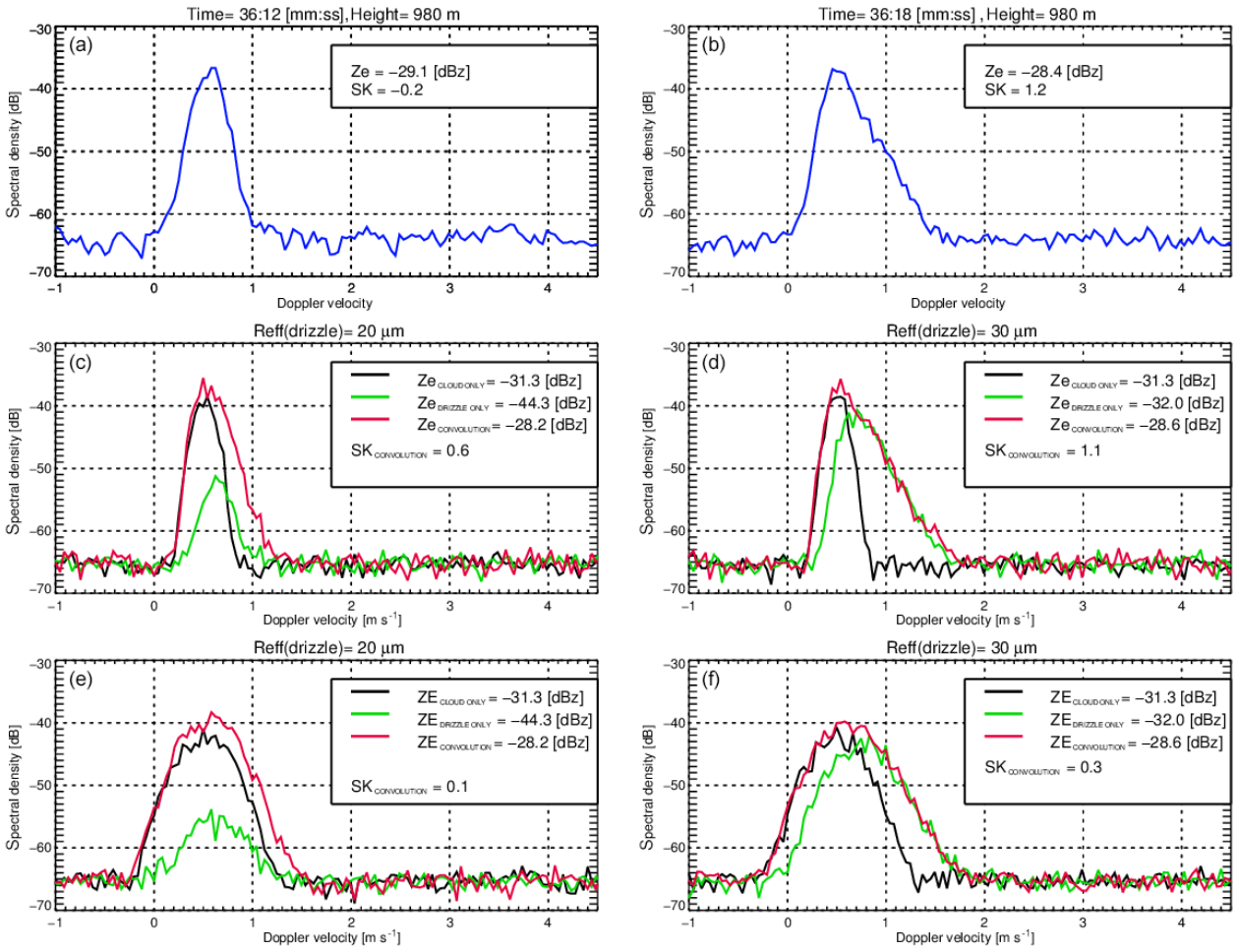

Figure 8. Comparison between simulated and observed spectra. Panels **(a)** and **(b)** show real Doppler spectra obtained during the drizzle case for nfft = 512 and $\Delta T = 2$ s in regions of early **(a, c, e)** and more mature drizzle development **(b, d, f)**. Panels **(c)** to **(f)** show examples of simulated Doppler spectra for cloud droplets (black), drizzle (green) and cloud+drizzle drops (red) for a low EDR of 3×10^{-4} m^2 s^{-3} **(c, d)** and high EDR of 5×10^{-3} m^2 s^{-3} **(e, f)**. Panels **(a)**, **(c)** and **(e)** show spectra for a lognormal drizzle DSD with effective radius of 20 µm while **(b)**, **(d)** and **(f)** are calculated with a drizzle effective radius of 30 µm.

3.2.2 Impact of integration time and spectral resolution on simulated moments

Statistical distributions of simulated moments of the convoluted spectra from cloud and drizzle droplets are shown in Figs. 9 and 10. Simulated reflectivities correspond to the highest Z_e values observed (Fig. 6) and lie in a narrow interval. This is because we only assumed a single DSD of cloud and drizzle drops and only vary EDR and vertical air motion. When smaller averaging time and larger n_{fft} are used, the variability increases due to the small number of spectral averages. As in the observations (compare Figs. 9d, e, f and 10d, e, f with Fig. 6d, e, f), V_d is not affected by n_{fft} and averaging time but it appears to be biased towards positive velocities. This is not surprising considering that we assume the distribution of V_d previous to our I/Q experiment as a proxy for vertical air motion and that this distribution is biased towards larger positive velocities due to sedimenting drizzle drops. As for the observations, the mean values of S_w increase with longer integration time while the n_{fft} has a negligible effect. In contrast to the observations, the simulated S_k values are only positive and range up to 1.5. We explain this effect to the use of the specific drizzle DSDs. These large positive values of simulated skewness with PAMTRA are a result of the long tail of the selected shape for the drizzle DSD. While this shape might be typical for mature drizzle distributions, the distribution is expected to be more narrow during the early stages of drizzle production (i.e., near cloud top). The absence of negative values is attributed to three factors. During heavy drizzle conditions a reversal of the sign of the S_k is expected; however, here this is not the case because the selected drizzle DSDs do not cause the drizzle spectrum to exceed the cloud droplet spectrum. The second factor is the absence of nonlinear horizontal shear of the vertical air

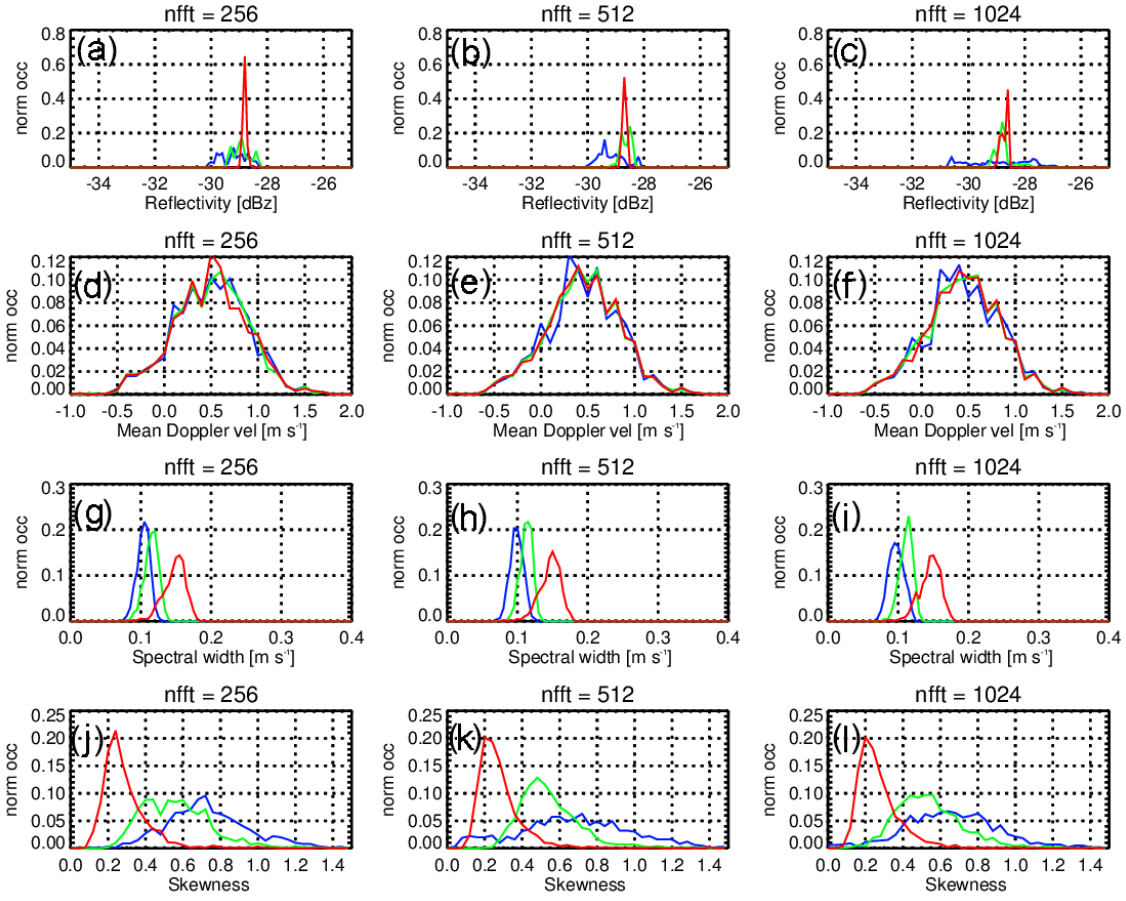

Figure 9. Distributions of simulated radar moments Z_e, V_d, S_w, S_k (from top to bottom) normalized by the total number of simulations ($N = 1000$) for cloud and drizzle droplets using $R_{eff,d} = 20\,\mu m$ and $r_{LWC} = 2.0\,\%$. The moments are derived for averaging times of 10 s (red), 2 s (green) and 0.4 s (blue) and different n_{fft}(increasing from left to right).

motion in the PAMTRA simulator. This is discussed in detail in Luke and Kollias (2013). Finally, low signal-to-noise conditions can increase the uncertainty of the measured radar Doppler spectra skewness and thus give rise to negative radar Doppler spectra skewness values, i.e., like those observed by JOYRAD-35.

The distributions of simulated S_k values show smaller values of skewness using 20 µm effective radius for drizzle (Fig. 9) compared to the simulation for $R_{eff} = 30\,\mu m$ (Fig. 10), and a shift of the S_k distributions to larger values for smaller ΔT is found in both simulations. This effect cannot be seen as clearly in the distributions of observed S_k values (Fig. 6), even if the occurrence of large values of skewness is reduced for longer integration times. In the observations, the natural variability of the skewness is so high that averaging does not help to detect a variation of the mean value with integration time. The almost constant mean value of skewness (see Table 6) is probably due to the presence of the negative skewness values, which are not reproduced in the simulations. In the simulations, the same drop size distribution is used for all the averaging times, reducing the variability of the signal. Smoothing effects due to longer averaging times are expected to reduce the mean value of skewness for longer ΔT in the simulations, as it is found. For longer averaging times, more spectra with individual random perturbations are averaged together. Consequently, the signal-to-noise ratio is enhanced, which can reveal signals previously hidden below the mean noise level. The resulting Doppler spectrum has a more symmetrical shape with skewness closer to zero. In order to reduce the impact of the natural variability of the skewness signal, we focus on a region of coherent skewness, selecting an area where the skewness signature appears to be induced by the microphysics only. If we focus the analysis on cloud regions with spatiotemporal coherent positive skewness structures as shown in Fig. 11, we obtain distributions of skewness values for the three different integration times and a spectral resolution of nfft = 256 as shown in the upper panel of Fig. 11. Despite the reduced number of observations contained in the selected region, a comparison with Fig. 10 seems to indicate that the range of observed skew-

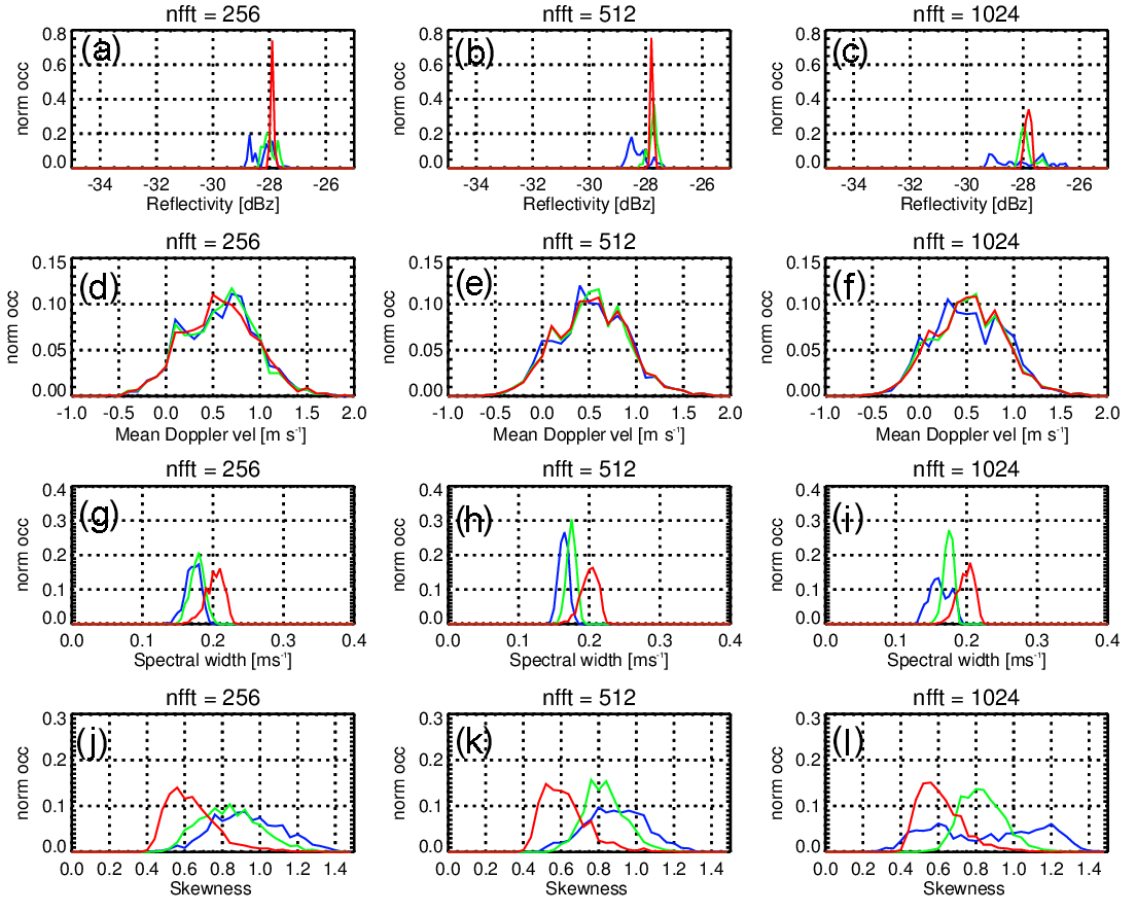

Figure 10. Similar to Figure 9, but using $R_{\mathrm{eff,d}} = 30\,\mu\mathrm{m}$ and $r_{\mathrm{LWC}} = 0.5\,\%$.

ness values now better matches the simulations. In addition, the shifting of the peak towards positive skewness with decreasing averaging time as well as a corresponding increased occurrence of positive extremes in S_{k} closer resembles the simulations.

Overall, the simulated distributions reveal – in agreement with the observations – only a minor effect of n_{fft} on the S_{k} distributions. The distributions of simulated moments reproduce the main effects induced by integration time and spectral resolution on the moments estimations, confirming the choice of 256 n_{fft} length and 2 s integration time as optimal settings for drizzle detection.

3.2.3 Impact of beam width and turbulence

We further analyze our findings for different microphysical situations as a function of assumed level of turbulence and the radar antenna beam width using a fixed integration time of 2 s (Fig. 12). Under low-turbulence conditions and a very small r_{LWC}, the skewness shows very high values, which tend to decrease for larger r_{LWC} (Fig. 12a). In fact, increasing the liquid amount of drizzle generates a more pronounced drizzle peak which results in a spectrum more similar to a Gaussian shape and is less asymmetric than in the case of low r_{LWC} (Fig. 12c, d, e). The value of the skewness observed also depends on whether the drizzle effective radius is large enough to introduce a sufficient asymmetry on the right of the cloud peak (see Fig. 12c, d, e). If the effective radius of the drizzle is too small (i.e., for 10 µm effective radius in Fig. 12c), the drizzle contribution is concealed by the cloud part and the skewness will be just slightly positive for increasing r_{LWC}. Figure 12a also shows that under low-turbulence conditions the skewness signal generated by the presence of drizzle and characterized by an effective radius of at least 20 µm is always greater than 0.4, which is the detection limit estimated for the observations (see Sect. 3.1). This indicates that there is potential for the detection of drizzle onset of 20 µm effective radius within the cloud in the presence of low turbulence. In the presence of high turbulence conditions, all skewness values are damped with respect to the ones derived in low turbulence conditions (Fig. 12b). Here, most of the expected skewness values are below the noise threshold and only drizzle of larger than 40 µm can be detected. Figure 12a and b show the strong dampening impact of turbulence on skew-

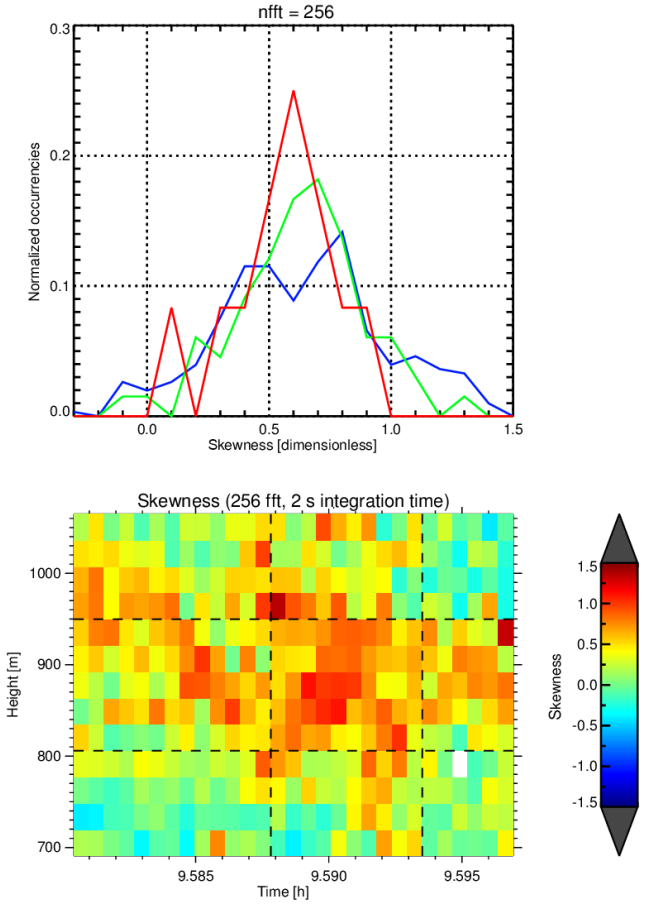

Figure 11. Selection of positive skewness values due to drizzle fingerprint in the observations from the case study of the 24 June 2015. Upper panel: distributions of skewness observed values derived using a spectral resolution of 256 and integration time of 10 s (red), 2 s (green) and 0.4 s (blue). Lower panel: box of positive skewness values selected for the analysis.

ness observations, which is not compensated by the choice of adopting smaller beam widths. In fact, a smaller beam width allows the detection of only slightly higher skewness values in both turbulence conditions, compared to the larger beam width. However, the gain due to the beam width appears more evident for effective radii around 20–30 µm, underlining the importance of narrow beam widths for the accuracy of skewness estimation when low-turbulence conditions are present.

4 Conclusions

In this study, we quantified how integration time and spectral resolution influence moment estimation in the specific context of liquid clouds and drizzle onset. Once certain radar settings (such as a long integration time) have been set by the user, a more detailed analysis might be impossible and potentially interesting microphysical signatures might be lost. Therefore, it is vital to carefully choose radar settings in order to establish high-quality datasets of cloud radar observations in drizzle clouds and to enable future comparisons of long-term datasets obtained with different radar systems and at different sites. This requires an optimal compromise between limiting the demands on data storage and conserving relevant microphysical information.

We analyzed consecutive zenith-pointing radar observations for two case studies of liquid nondrizzling and drizzling clouds. We found that, in the specific context of liquid clouds and drizzle initiation, longer integration times mainly modify spectral width and skewness, leaving the other moments hardly altered. For drizzle applications, we found an uncertainty on skewness measurements to be of the order of 0.4.

Simulations performed with a radar forward simulator, which allows to explicitly define the state of drizzle, are in general agreement with observations. Spectral width is increased by longer integration times due to the broadening of the spectrum shape. In the observations, this effect is attributed to turbulence and is confirmed by simulations. Skewness undergoes a reduction of the occurrence of larger values when longer integration times are used. From the simulations we conclude that both an increase in S_w and a reduction in S_k in the case of the 10 s average can lead to significantly different microphysical interpretations with respect to drizzle water content and effective radius (Fig. 12) compared to shorter integration times.

For the specific application of drizzle detection, we found the integration time of 2 s to be an optimal compromise: on the one hand, it limits the turbulence-induced effects on S_w and S_k at longer integration times, while on the other hand, it guarantees a minimum required level of sensitivity (a factor of 5 in terms of longer integration times corresponds to an increase in sensitivity of 3.5 dB), which is not achieved with shorter integration times. We also concluded that FFT lengths have a smaller impact on the moment estimations, and thus on the microphysical interpretation of the drizzle signal: 256 FFT length seems appropriate for calculating moments with no significant differences compared to 512 or 1024.

Moreover, simulations provided additional insight into the microphysical interpretation of the skewness signatures observed: in low (high)-turbulence condition, only drizzle bigger than 20 µm (40 µm) can generate skewness values above the noise level. Higher skewness values are also obtained in simulations when smaller beam widths are adopted in contrast to skewness values derived in the same conditions but with larger beam widths.

In summary, this experiment presents a first step towards the optimal choice of radar parameter settings when retrieving drizzle parameters exploiting higher Doppler spectra moments. One clear limitation is the restriction to two short case studies due to the extremely large amount of data to be handled when working with raw I/Q measurements. In this context, the agreement between simulations and observations is even more convincing, because the large amount

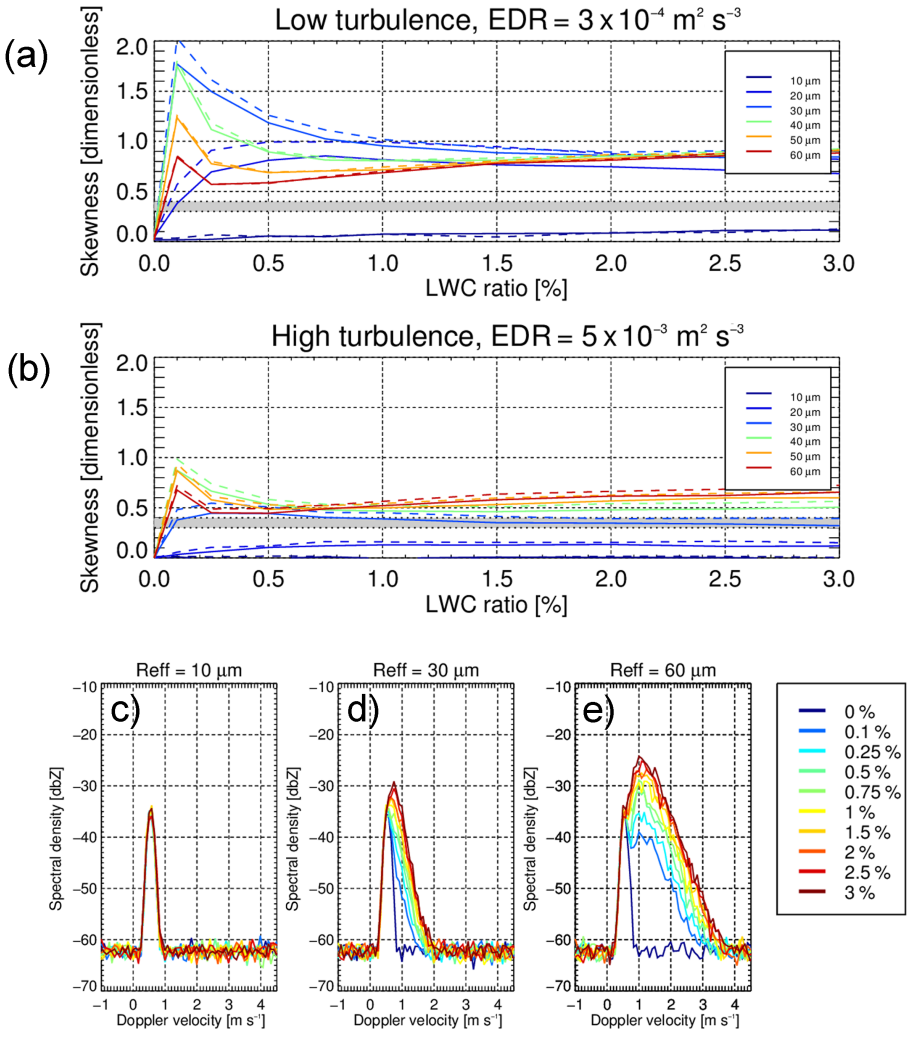

Figure 12. Panels **(a)** and **(b)**: skewness of the convoluted spectrum of cloud and drizzle drop size distributions as a function of r_{LWC} for different drizzle effective radii and low EDR **(a)** and high EDR **(b)**. Simulations have been performed using 0.6° (solid line) and 0.3° (dashed line) radar beam widths. The grey bar represents the uncertainty of the skewness observations. **(c)**, **(d)** and **(e)**: Doppler spectra corresponding to the various r_{LWC} obtained using drizzle effective radii of 10 **(c)**, 20 **(d)** and 30 µm **(e)**.

of simulations performed (1000) underline and confirm what was observed during the short observation period. The developed methodology, showing how such requirements can be derived in general, will be applicable to other cloud types and microphysical processes. This can verify how radar settings can impact the identification of spectral features like bimodalities found in mixed-phase clouds due to the presence of supercooled liquid water, ice, snow and rimed particles (Shupe et al., 2004; Verlinde et al., 2013; Kalesse et al., 2015).

Data availability. All data used for this study are available on request from the corresponding author.

The Supplement related to this article is available online at doi:10.5194/amt-10-1783-2017-supplement.

Competing interests. The authors declare that they have no conflict of interest.

Acknowledgements. This research has received funding through Initial Training for Atmospheric Remote Sensing (ITARS; www.itars.net), European Union Seventh Framework Programme (FP7/2007–2013): People, and ITN Marie Curie Actions Programme (2012–2016) under Grant Agreement 289923 as well as from ACTRIS-2 (www.actris.eu) in the European Union's Horizon 2020 research and innovation programme under grant agreement no. 654109. Additionally, the cloud radar data management and interpretation have been funded by the research initiative High Def-

inition Clouds and Precipitation for advancing Climate Prediction HD(CP)2 I under grants FKZ01LK1209A and FKZ01LK1209B (PI Anne Hirsikko) funded by the German Ministry for Education and Research (BMBF). Furthermore, the Transregional Collaborative Research Center TR32 Patterns in Soil-Vegetation-Atmosphere Systems, funded by the German Science Foundation (DFG), has contributed significantly to the maintenance of the cloud radar. M. Maahn was supported by funding from the US Department of Energy Atmospheric System Research (ASR) program (award DE-SC0013306). The authors would like to thank the anonymous reviewers for their helpful comments which improved the quality of the manuscript. The authors would like to thank all scientists taking part in the regular "cloud Doppler radar spectra skype meetings" for their interest and contribution regarding this work and, in addition, especially Susanne Crewell, Gabriele Corbetta, Emiliano Orlandi, Paloma Borque and Andrés Peréz.

Edited by: S. J. Munchak
Reviewed by: A. Loftus and two anonymous referees

References

Atlas, D., Srivastava, R., and Sekhon, R. S.: Doppler radar characteristics of precipitation at vertical incidence, Rev. Geophys., 11, 1–35, 1973.

Borque, P., Luke, E., and Kollias, P.: On the unified estimation of turbulence eddy dissipation rate using Doppler cloud radars and lidars, J. Geophys. Res.-Atmos., 121, 5972–5989, 2016.

Doviak, R. and Zrnic, D.: Doppler Radar & Weather Observations, Academic press, 2014.

Frisch, A., Fairall, C., and Snider, J.: Measurement of stratus cloud and drizzle parameters in ASTEX with a Kα-band Doppler radar and a microwave radiometer, J. Atmos. Sci., 52, 2788–2799, 1995.

Görsdorf, U., Lehmann, V., Bauer-Pfundstein, M., Peters, G., Vavriv, D., Vinogradov, V., and Volkov, V.: A 35-GHz polarimetric Doppler radar for long-term observations of cloud parameters-Description of system and data processing, J. Atmos. Ocean. Tech., 32, 675–690, 2015.

Gossard, E.: Measurement of cloud droplet size spectra by Doppler radar, J. Atmos. Ocean. Tech., 11, 712–726, 1994.

Gossard, E. E., Snider, J., Clothiaux, E., Martner, B., Gibson, J. S., Kropfli, R., and Frisch, A.: The potential of 8-mm radars for remotely sensing cloud drop size distributions, J. Atmos. Ocean. Tech., 14, 76–87, 1997.

Hildebrand, P. H. and Sekhon, R.: Objective determination of the noise level in Doppler spectra, J. Appl. Meteorol., 13, 808–811, 1974.

Illingworth, A., Hogan, R., O'connor, E. et al.: Cloudnet, B. Am. Meteorol. Soc., 88, 883–898, 2007.

Kalesse, H., Szyrmer, W., Kneifel, S., Kollias, P., and Luke, E.: Fingerprints of a riming event on cloud radar Doppler spectra: observations and modeling, Atmos. Chem. Phys., 16, 2997–3012, doi:10.5194/acp-16-2997-2016, 2016.

Khvorostyanov, V. I. and Curry, J. A.: Terminal velocities of droplets and crystals: Power laws with continuous parameters over the size spectrum, J. Atmos. Sci., 59, 1872–1884, 2002.

Kollias, P., Albrecht, B., Lhermitte, R., and Savtchenko, A.: Radar observations of updrafts, downdrafts, and turbulence in fair-weather cumuli, J. Atmos. Sci., 58, 1750–1766, 2001.

Kollias, P., Albrecht, B. A., Clothiaux, E. E., Miller, M. A., Johnson, K. L., and Moran, K. P.: The Atmospheric Radiation Measurement program cloud profiling radars: An evaluation of signal processing and sampling strategies, J. Atmos. Ocean. Tech., 22, 930–948, 2005.

Kollias, P., Clothiaux, E., Miller, M., Albrecht, B., Stephens, G., and Ackerman, T.: Millimeter-wavelength radars, B. Am. Meteorol. Soc., 88, 1608–1624, 2007a.

Kollias, P., Miller, M. A., Luke, E. P., Johnson, K. L., Clothiaux, E. E., Moran, K. P., Widener, K. B., and Albrecht, B. A.: The Atmospheric Radiation Measurement Program cloud profiling radars: Second-generation sampling strategies, processing, and cloud data products, J. Atmos. Ocean. Tech., 24, 1199–1214, 2007b.

Kollias, P., Rémillard, J., Luke, E., and Szyrmer, W.: Cloud radar Doppler spectra in drizzling stratiform clouds: 1. Forward modeling and remote sensing applications, J. Geophys. Res.-Atmos., 116, 1–14, 2011a.

Kollias, P., Szyrmer, W., Rémillard, J., and Luke, E.: Cloud radar Doppler spectra in drizzling stratiform clouds: 2. Observations and microphysical modeling of drizzle evolution, J. Geophys. Res.-Atmos., 116, 1–14, 2011b.

Kollias, P., Tanelli, S., Battaglia, A., and Tatarevic, A.: Evaluation of EarthCARE cloud profiling radar Doppler velocity measurements in particle sedimentation regimes, J. Atmos. Ocean. Tech., 31, 366–386, 2014.

Kollias, P., Clothiaux, E. E., Ackerman, T. P., Albrecht, B. A., Widener, K. B., Moran, K. P., Luke, E. P., Johnson, K. L., Bharadwaj, N., Mead, J. B., Miller, M. A., Verlinde, J., Marchand, R. T., and Mace, G. G.: Development and Applications of ARM Millimeter-Wavelength Cloud Radars, Meteor. Mon., 57, 1–19, 2016.

Löhnert, U., Kneifel, S., Battaglia, A., Hagen, M., Hirsch, L., and Crewell, S.: A multisensor approach toward a better understanding of snowfall microphysics: The TOSCA project, B. Am. Meteor. Soc., 92, 613–628, 2011.

Löhnert, U., Schween, J., Acquistapace, C., Ebell, K., Maahn, M., Barrera-Verdejo, M., Hirsikko, A., Bohn, B., Knaps, A., O'connor, E., Simmer, C., Wahner, A., and Crewell, S.: JOYCE: Jülich observatory for cloud evolution, B. Am. Meteor. Soc., 96, 1157–1174, 2015.

Luke, E. P. and Kollias, P.: Separating cloud and drizzle radar moments during precipitation onset using Doppler spectra, J. Atmos. Ocean. Tech., 30, 1656–1671, 2013.

Maahn, M.: Exploiting vertically pointing Doppler radar for advancing snow and ice cloud observations, Ph.D. thesis, Universität zu Köln, http://kups.ub.uni-koeln.de/6002/, last access: 13 March 2015.

Maahn, M. and Löhnert, U.: Potential of Higher-Order Moments and Slopes of the Radar Doppler Spectrum for Retrieving Microphysical and Kinematic Properties of Arctic Ice Clouds, J. Appl. Meteor. Climatol., 56, 263–282, doi:10.1175/JAMC-D-16-0020.1, 2017.

Maahn, M., Löhnert, U., Kollias, P., Jackson, R. C., and McFarquhar, G. M.: Developing and evaluating ice cloud parameteri-

zations for forward modeling of radar moments using in situ aircraft observations, J. Atmos. Ocean. Tech., 32, 880–903, 2015.

Mie, G.: Beiträge zur Optik trüber Medien, speziell kolloidaler Metallösungen, Ann. Phys., 330, 377–445, doi:10.1002/andp.19083300302, 1908.

Miles, N. L., Verlinde, J., and Clothiaux, E. E.: Cloud droplet size distributions in low-level stratiform clouds, J. Atmos. Sci., 57, 295–311, 2000.

O'Connor, E. J., Hogan, R. J., and Illingworth, A. J.: Retrieving stratocumulus drizzle parameters using Doppler radar and lidar, J. Appl. Meteorol., 44, 14–27, 2005.

Shupe, M. D., Kollias, P., Matrosov, S. Y., and Schneider, T. L.: Deriving mixed-phase cloud properties from Doppler radar spectra, J. Atmos. Ocean. Tech., 21, 660–670, 2004.

Tridon, F. and Battaglia, A.: Dual-frequency radar Doppler spectral retrieval of rain drop size distributions and entangled dynamics variables, J. Geophys. Res.-Atmos., 120, 5585–5601, 2015.

Uttal, T. and Kropfli, R. A.: The effect of radar pulse length on cloud reflectivity statistics, J. Atmos. Ocean. Tech., 18, 947–961, 2001.

Verlinde, J., Rambukkange, M. P., Clothiaux, E. E., McFarquhar, G. M., and Eloranta, E. W.: Arctic multilayered, mixed-phase cloud processes revealed in millimeter-wave cloud radar Doppler spectra, J. Geophys. Res.-Atmos., 118, 199–213, 2013.

Zrnic, D. S.: Simulation of weatherlike Doppler spectra and signals, J. Appl. Meteorol., 14, 619–620, 1975.